

RSC Advances



This is an *Accepted Manuscript*, which has been through the Royal Society of Chemistry peer review process and has been accepted for publication.

Accepted Manuscripts are published online shortly after acceptance, before technical editing, formatting and proof reading. Using this free service, authors can make their results available to the community, in citable form, before we publish the edited article. This *Accepted Manuscript* will be replaced by the edited, formatted and paginated article as soon as this is available.

You can find more information about *Accepted Manuscripts* in the [Information for Authors](#).

Please note that technical editing may introduce minor changes to the text and/or graphics, which may alter content. The journal's standard [Terms & Conditions](#) and the [Ethical guidelines](#) still apply. In no event shall the Royal Society of Chemistry be held responsible for any errors or omissions in this *Accepted Manuscript* or any consequences arising from the use of any information it contains.

Electrochemical Sensing of Nitrite using Copper-Titanium Oxide

Composite Derived from Hexanuclear Complex

Muhammad Ali Ehsan,^a Rabia Naeem,^b Vickie McKee,^c Abbas Hakeem Saeed,^a Alagarsamy Pandikumar,^d Nay Ming Huang,^d Muhammad Mazhar,^{b*}

[a] Center of Research Excellence in Nanotechnology (CENT), King Fahd University of Petroleum & Minerals, Saudi Arabia.

[b]*Department of Chemistry, Faculty of Science, University of Malaya, Lembah Pantai, 50603-Kuala Lumpur, Malaysia.

[c] School of Chemical Sciences, Dublin City University, Glasnevin, Dublin 9, Ireland

[d] Department of Physics, Faculty of Science, University of Malaya, Lembah Pantai, 50603-Kuala Lumpur, Malaysia.

**Corresponding author's e-mail: mazhar42pk@yahoo.com, Tel.: +60379674269;*

Fax: +60379674193

Abstract

A hexanuclear copper-titanium complex $[\text{Cu}_2\text{Ti}_4(\text{O})_2(\text{OH})_4(\text{TFA})_8(\text{THF})_6]\cdot\text{THF}$ (**1**) (where TFA = trifluoroacetato, THF = tetrahydrofuran) has been identified on the treatment of copper (II) acetate with titanium (IV) isopropoxide and trifluoroacetic acid in THF. The physicochemical properties of complex (**1**) have been inspected by melting point, microanalysis, attenuated total reflectance Fourier transform infrared spectroscopy, thermogravimetry and single crystal X-ray analysis. The “single source” potential of complex (**1**) has been explored by a solution based aerosol assisted chemical vapor deposition method to fabricate CuO-2TiO₂ composite oxide thin

films on fluorinated tin oxide (FTO) conducting glass substrate at 550 °C in air ambient. Thin film characterization such as X-ray powder diffraction, Raman spectroscopy and X-ray photoelectron spectroscopy, energy dispersive X-ray and scanning electron microscopic analyses confirm the evolution of crystalline CuO: 2TiO₂ composite having spherical morphologies with clear grain boundaries and in high purity. Further the well-characterized film electrode was investigated for electrochemical detection of nitrite ions (NO₂⁻). The fabricated CuO-2TiO₂ electrode showed peak at +1.0 V due to the oxidation of NO₂⁻ ions. The limit of detection (LoD) was found to be 0.0166 μM with the linear range of 10 to 200 μM. Moreover, this present sensor is more selective towards NO₂⁻ ions and it did not show any response to other interfering species. This CuO-2TiO₂ electrode is a potential candidate for the selective and sensitive detection of toxic NO₂⁻ ions towards monitoring the NO₂⁻ ions levels in natural water sources for environmental remediation application.

1. Introduction

Titanium dioxide (TiO₂) is known for its numerous and diverse applications which range from common products such as sunscreens¹, to advanced devices, such as photovoltaic cells², photocatalytic degradation of pollutants³, water purification⁴ and biomedical implementation.⁵ The combination of TiO₂ with other transition metal oxides produces materials that exhibit versatile properties and have revolutionized many technological areas specially the energy^{6,7} and environmental sectors.^{8,9} The importance and variety of these applications have spurred enormous interest and substantial advances in the fabrication, characterization, and fundamental understanding of TiO₂ based nanomaterials in the past decades.^{10,11,12}

Titania based copper oxide (CuO-TiO₂) nanocomposite offers promising photocatalytic performances both in H₂ generation¹³ and organic pollutant degradation.¹⁴ Synthetic methods

have a central role in the performance of a material therefore several efforts to produce copper oxide-titania composite oxides in variety of shapes, designs and architectures have greatly improved its photocatalytic efficiency.^{15,16} Recently, Wei Ho et al. created unique wheat grain like textured of CuO/TiO₂ composite by electrospinning technique.¹⁷ Wang's group prepared CuO/TiO₂ composites by six different methods such as simple wet impregnation, ethanol impregnation, stepwise impregnation, in situ sol-gel, chemical adsorption decomposition, and composite precipitation and compared their photocatalytic performances.¹⁸

Among the various synthetic strategies, single molecular precursor (SMP) based chemical vapor deposition method is less explored for the formation of such composite oxide systems. This synthetic route is considered very effective for the synthesis of bi and multicomponent advanced functional oxide materials with high crystallinity, spatially oriented nanostructure, excellent control over homogeneity, stoichiometry and reproducibility of the final product at relatively less drastic environments.^{19,20} However, these targets can only be met by using a well-defined heterobimetallic compound with adequate volatility and thermal stability which can qualify the CVD precursor criteria for thin film deposition.

Previously, We developed few Cu-Ti heterometallic complexes including [Ti₄(dmae)₆(μOH)(μ-O)₆Cu₆(benzoate)₉]²¹, [Ti₄(dmae)₆(μ-OH)(μ-O)₆Cu₆(2-methylbenzoate)₉]²¹, [Ti₄(dmae)₆(μ-OH)(μ-O)₆Cu₆(OAc)₉H₂O]²² by taking advantage of bifunctional *N,N*-dimethylaminoethanolato (dmae) as a bridging moiety between two hetero metal centers. The implementation of these heterometallic coordination compounds in aerosol assisted chemical vapor deposition (AACVD) technique resulted in formation of Cu₃TiO₄/TiO₂ composite oxide thin films. However, the modifications in heterometallic assemblies can be made by introducing a different ligand group

which can tune the physicochemical properties of the heteronuclear complex to create novel materials.

In the present work a new Cu-Ti heterometallic assembly is constructed through a well known trifluoroacetato (CF_3COO^-) bridging group. The strategy to use fluorinated ligands presents some extra advantages over the amino alcohol ligands. The hydrophobic nature of the fluoro groups can be exploited to control the hydrolysis rates of many moisture-sensitive complexes, for example, alkoxide derivatives, and thereby design more hydrolytically stable and hence easy to handle precursors.^{23,24} Also, the enhanced strength of the carbon-fluorine bond over the carbon-hydrogen bond leads to greater thermal stability. The presence of strongly electron-withdrawing CF_3 groups in alpha positions generates a less basic O donor site, making these ligands far less π donating than aminoalcohol ligands. As a result, low-nuclearity complexes are generally formed, which are more soluble and volatile. The use of fluorinated functional ligands also favorably modify the properties of metal-organic precursors for materials processing. A fluorinated ligand not only modifies the physicochemical properties, but also alters the reactivity of the resulting metallic derivatives.^{23,25}

Current work details about synthesis, structural and thermal investigations of the heterobimetallic complex $[\text{Cu}_2\text{Ti}_4(\text{O})_2(\text{OH})_4(\text{TF})_8(\text{THF})_6]\cdot\text{THF}$ (**1**) (where TFA = trifluoroacetato, THF = tetrahydrofuran) and its utilization as molecular precursor in AACVD technique for the development of CuO-2TiO_2 composite films on fluorinated tin oxide (FTO) conducting glass substrate at the relatively low temperature of 550 °C. Thin films deposited from two different deposition (methanol and ethanol) solutions of (**1**) were examined by X-ray diffraction (XRD), Raman spectroscopy, scanning electron microscopy (SEM), energy dispersive X-ray (EDX) and X-ray photoelectron spectroscopy (XPS) for the evaluation of their phase, structural, textural

and compositional properties. Further, the fabricated CuO-2TiO₂ electrode used for electrochemical detection of nitrite (NO₂⁻) ions since high level of NO₂⁻ are detrimental to the human body that causes methemoglobinemia, and blue baby syndrome.^{26,27}

2. Experimental

2.1 Material and methods

All synthetic reactions were carried out under an inert atmosphere of dry argon using Schlenk tubes fitted with vacuum line and hot plate arrangements. The solvent was rigorously dried over sodium benzophenone and distilled immediately before use. Copper(II) acetate monohydrate (Cu(CH₃COO)₂·H₂O), titanium(IV) isopropoxide (Ti(OCH(CH₃)₂)₄) and trifluoroacetic acids (CF₃COOH) were purchased from Aldrich Chemical Co. The reagents were used as received. The melting point was determined in a capillary tube using an electrothermal melting point apparatus; model MP.D Mitamura Riken Kogyo (Japan). The elemental analyses were performed using Leco CHNS 932. Fourier transform infra-red (FT-IR) spectrum was recorded on a single reflectance ATR instrument (4000–400 cm⁻¹, resolution 4 cm⁻¹). The controlled thermal analysis was investigated using a Perkin Elmer TGA 4000 thermogravimetric analyzer with a computer interface. The thermal measurements were carried out in a ceramic crucible under an atmosphere of flowing nitrogen (50 mL min⁻¹) with a heating rate of 10 °C min⁻¹.

2.2 Synthesis of [Cu₂Ti₄(O)₂(OH)₄(TFA)₈(THF)₆]·THF (1)

Complex (1) was prepared by mixing stoichiometric amounts of 0.50g (2.50 mmol) of Cu(CH₃COO)₂·H₂O and 1.49mL (5.03mmol) of Ti(OCH(CH₃)₂)₄ followed by the addition of 1.14mL (10.05mmol) of CF₃COOH in 25mL of THF in a 50mL Schlenk tube. The reaction mixture was stirred for 4hours and solvent was evacuated under vacuum to

obtain a green powder which was dissolved in THF. The resulting transparent solution was cannula-filtered and placed at room temperature for overnight to obtain green block shape crystals of precursor (**1**) in 70% yield. Melting point, elemental analysis, IR and TGA data of complex (**1**) is comprised in table 1.

Table 1. Melting point, elemental analysis, IR and TGA data of complex (**1**)

Complex	Melting point (°C)	Elemental analysis Found (Calc.) %		IR frequencies, (cm ⁻¹)			TGA data Temp (°C) (% wt. loss)
		C	H	v(C=O)	v(C-O)	C-F	
(1)	225	27.96	2.87	1671, 1471	1197	1147	1 st : 51-134 (11.1)
		(28.89)	(3.17)				2 nd : 139-240 (25.8)
							3 rd : 241-277 (14.0)
							4 th step: 280-500 (22.3)
							Residue at 500 (26.8)
							(Cal. for CuO-2TiO ₂ 26.18%).

2.3 Single-crystal X-ray crystallography

The data were collected at 150(2)K on a Bruker-Nonius Apex II CCD diffractometer using MoK_α radiation ($\alpha = 0.71073\text{\AA}$) and were corrected for Lorentz-polarisation effects and absorption (SADABS).²⁸ The structure was solved by dual space methods (SHELXT)²⁹ and refined on F² using all the reflections (SHELXL-2014)³⁰. The central section, comprising most of the molecule is disordered and was modelled with 50% occupancy of two positions related by a centre of symmetry (reduction of the space group symmetry did not reduce the disorder). Additionally some disorders in the THF molecules were modelled as overlapping conformations (see supplementary data). All the non-hydrogen atoms were refined using anisotropic atomic displacement parameters and hydrogen atoms were inserted at calculated positions using a riding model. Parameters for data collection and refinement are summarised in Table 2.

Table 2. Crystal data and refinement parameters for $[\text{Cu}_2\text{Ti}_4(\text{O})_2(\text{OH})_4(\text{TF})_8(\text{THF})_6]\cdot\text{THF}$

(1)

$\text{C}_{40}\text{H}_{52}\text{Cu}_2\text{F}_{24}\text{O}_{28}\text{Ti}_4\cdot\text{C}_4\text{H}_8\text{O}$	$V = 6863.3 (7) \text{ \AA}^3$
$M_r = 1827.60$	$Z = 4$
Orthorhombic, $Pbca$	Mo $K\alpha$ radiation, $\lambda = 0.71073 \text{ \AA}$
$a = 18.8071 (11) \text{ \AA}$	$\mu = 1.20 \text{ mm}^{-1}$
$b = 17.3656 (10) \text{ \AA}$	$T = 150 \text{ K}$
$c = 21.0146 (12) \text{ \AA}$	$0.43 \times 0.32 \times 0.24 \text{ mm}$
$R[F^2 > 2\sigma(F^2)] = 0.067$	59386 measured reflections
$wR(F^2) = 0.217$	7057 independent reflections
$S = 1.01$	4097 reflections with $I > 2\sigma(I)$
$\Delta\rho_{\text{max}} = 0.65 \text{ e \AA}^{-3}$	1810 restraints
$\Delta\rho_{\text{min}} = -0.67 \text{ e \AA}^{-3}$	910 parameters

2.4 AACVD studies

Following our previous work^{19, 20}, AACVD was used to fabricate $\text{CuO}\cdot 2\text{TiO}_2$ composite oxide thin films from precursor (1) on commercially available FTO coated conducting glass substrates. Before starting the deposition experiments, the FTO coated glass was cut ($1 \times 2 \text{ cm}^2$) and ultrasonically cleaned with doubly distilled water, acetone, iso-propanol and ethanol prior to use. The substrates slides were then placed inside a reactor tube and furnace (CARBOLITE, Model No. 10/25/130) ($6''\text{L} \times 1''\text{D}$) was heated up to a deposition temperature ($550 \text{ }^\circ\text{C}$) for 10 min. Deposition experiments were conducted using 20 mL of 0.1 M solution of precursor (1) in two different solvents viz. methanol and ethanol. In a typical deposition experiment, the precursor solution was taken in a 50 mL round bottom flask which was immersed in water bath above the piezoelectric modulator of an ultrasonic humidifier (Model No. Cool Mist-plus serial No. ADV-CMP-85956). Air at a flow rate of 100 mL min^{-1} was used as the carrier gas and the

flow rate was controlled by an LIX linear flow meter. The generated aerosol droplets were then transferred into the hot wall zone of the reactor by the carrier gas. Both the solvent and the precursor were evaporated and the precursor vapor reached the heated substrate surface where thermally induced reactions and subsequent film deposition took place.

2.5 Thin film analysis

The nature of phase and crystallinity of the films were characterized using a PANalytical, X'Pert HighScore diffractometer with primary monochromatic high intensity Cu-K α ($\lambda = 1.54184$ Å) radiation over Bragg angles ranging from 15 to 90° in a step size of 0.026° and the operating voltage and current were maintained at 30 kV and 40 mA respectively. After identification of the crystalline components or phases by “qualitative phase identification analysis” the diffraction patterns were processed using “quantification ” button located on the tool bare of the X'Pert HighScore Plus software to calculate the crystalline phase percentages in the product mixture. The procedure adopted for phase quantification was RIR-based quantitative analysis³¹, that measured the integrated intensity of the strongest peak in each phase and then, using the reference intensity ratio (RIR), basically a scaling factor, converted these intensity values to weight percent.^{32, 33}

Raman spectroscopic measurements were carried out on a Renishaw InVia Raman microscope and excitation was performed using the 514 nm line of Argon laser with a 0.01 mW output power. The surface morphology and chemical composition of the thin films were analysed by field-emission scanning electron microscope (Hitachi FESEM SU 8000) equipped with EDX spectrometer (INCA Energy 200, Oxford Inst.) operated at an accelerating voltage of 20 kV and a working distance of 9.2 mm. X-ray photoelectron spectroscopy of thin films were studied using an ULVAC-PHI Quantera II with a 32-channel Spherical Capacitor Energy Analyzer under

vacuum (1×10^{-6} Pa) using Monochromated Al K α radiation (1486.8eV) and natural energy width of 680meV. The carbonaceous C 1s line (284.6 eV) was used as a reference to calibrate the binding energies.

2.6. Electrochemical studies

A conventional three-electrode electrochemical cell system was used with PAR-VersaSTAT-3 Electrochemical Workstation (www.princetonappliedresearch.com) for these electrochemical studies at room temperature. The CuO–2TiO₂ electrode, Pt and Ag/AgCl were used as working, counter and reference electrodes, respectively. A 0.1 M phosphate buffer solution (PBS) with pH 7.2 was used as a supporting electrolyte for the electrochemical experiments and all the potentials are quoted against Ag/AgCl reference electrode unless otherwise mentioned.

3 Results and discussion

3.1 Preparation and characterization of complex (1)

The chemical interaction between diacetatocopper(II) and tetrakis(isopropoxy)titanium(IV) in the presence of trifluoroacetic acid yields a heterobimetallic complex $[\text{Cu}_2\text{Ti}_4(\text{O})_2(\text{OH})_4(\text{TF})_8(\text{THF})_6] \cdot \text{THF}$ (**1**). The isopropoxo and acetato groups attached to titanium and copper centres are completely exchanged by the stronger trifluoroacetato ligands as the reaction progresses in forward direction.

The complex (**1**) prepared in a good yield, has copper to titanium ratio of 1:2, is stable in air and finds high solubility in common organic solvents such as methanol, ethanol acetonitrile and tetrahydrofuran.

The heterometallic architecture of the complex (**1**) has been framed on the basis of elemental analysis, ATR-FTIR, and single crystal X-ray analyses as described in experimental section. The ATR-FTIR spectrum (SI. Figure 1) of complex (**1**) shows the presence of characteristic

vibrations of functional groups attached to the copper and titanium atoms. The typical symmetric and asymmetric $\nu(\text{C}=\text{O})$ absorptions of trifluoroacetato ligand arose at 1671 and 1471 cm^{-1} respectively. The difference in value of 208 cm^{-1} between symmetric and asymmetric $\nu(\text{C}=\text{O})$ absorption bands reveals the bidentate behaviour of the carboxylato group of trifluoroacetato ligand that is bonded to different metal centres.^{34, 35} Similarly, the peak at 1195 cm^{-1} confirms the presence of C–F bonds in complex (1).^{34, 35}

3.2 Molecular structure of complex $[\text{Cu}_2\text{Ti}_4(\text{O})_2(\text{OH})_4(\text{TF})_8(\text{THF})_6]\cdot\text{THF}$ (1)

The structure of (1) was solved in space group *Pbca*, and is disordered about the centre of symmetry. The core of the molecule consists of a tetrahedron of Ti(IV) ions (Figure 1). Each edge of the tetrahedron is bridged by an oxygen atom (O^{2-} or OH^-), generating a Ti_4O_6 adamantane-type cage. Four of the bridging species are hydroxo ions; the remaining two are oxo ions which are also coordinated to Cu(II) ions. The disorder arises from titanium ions occupying alternative sites, generating a second, overlapping adamantane with the oxygen atoms in the same positions (see Supplementary data).

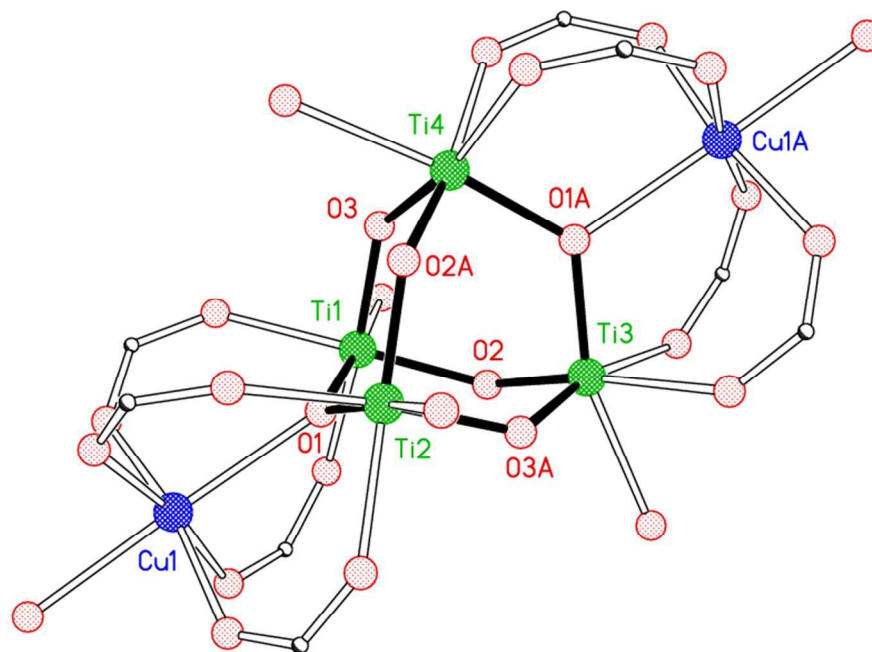


Figure 1: Perspective view of the core of **(1)**. CF_3COO^- ions are represented by OCO links; terminal O atoms represent THF molecules, bold bonds highlight the $\text{Ti}_4\text{O}_2(\text{OH})_4$ adamantane core. Atoms with suffix “A” generated by symmetry operation $1-x, 1-y, 1-z$.

Four trifluoroacetate (CF_3COO^-) ions are bonded to each copper ion; each trifluoroacetate also bridges to a titanium ion. All of the metal ions are six-coordinate, the last binding site being filled by one coordinated THF molecule for each metal ion (Figure 2). There is also a (disordered) non-coordinated THF solvate molecule in the lattice.

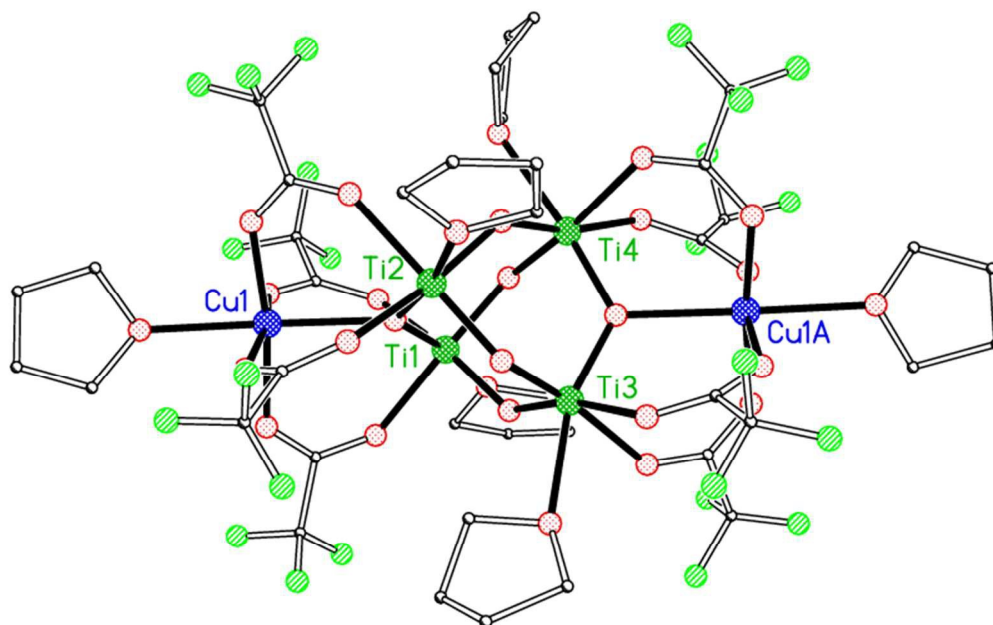


Figure 2: Perspective view of the $[\text{Cu}_2\text{Ti}_4(\text{O})_2(\text{OH})_4(\text{CF}_3\text{COO})_8(\text{THF})_6]$ (**1**) molecule. Bold bonds highlight the metal coordination spheres. Disorder and H atoms are omitted for clarity.

3.3 Thermal (TG/DTG) analysis of complex (**1**)

The thermal decomposition behaviour of the complex (**1**) was studied by simultaneous thermogravimetric (TG) and derivative thermogravimetric (DTG) analysis under an inert dinitrogen atmosphere with a flowing rate of $25 \text{ cm}^3 \text{ min}^{-1}$ and a heating rate of $10 \text{ }^\circ\text{C min}^{-1}$ and the results are presented in Figure 3. The TG/DTG curves impart that thermal degradation of (**1**) completes in four continuous weight loss steps and maximum heat intakes sequentially occur at 81, 225, 250 and 306 $^\circ\text{C}$ giving weight loss of 11.1 %, 25.8%, 14.0%, and 22.3% respectively. The thermal decay process in (**1**) ends at 500 $^\circ\text{C}$ leaving an invariable residue that amounts to 26.80 % of its original mass. The weight of the residue (26.18%) reasonably accords with the formation of the expected 1:2 CuO:

TiO₂ composite oxide material from (1). Further sintering of the observed residue to the higher temperature of 900 °C did not experience any change in weight, suggesting that (1) decomposes quantitatively to endow CuO-2TiO₂ as a stable final product.

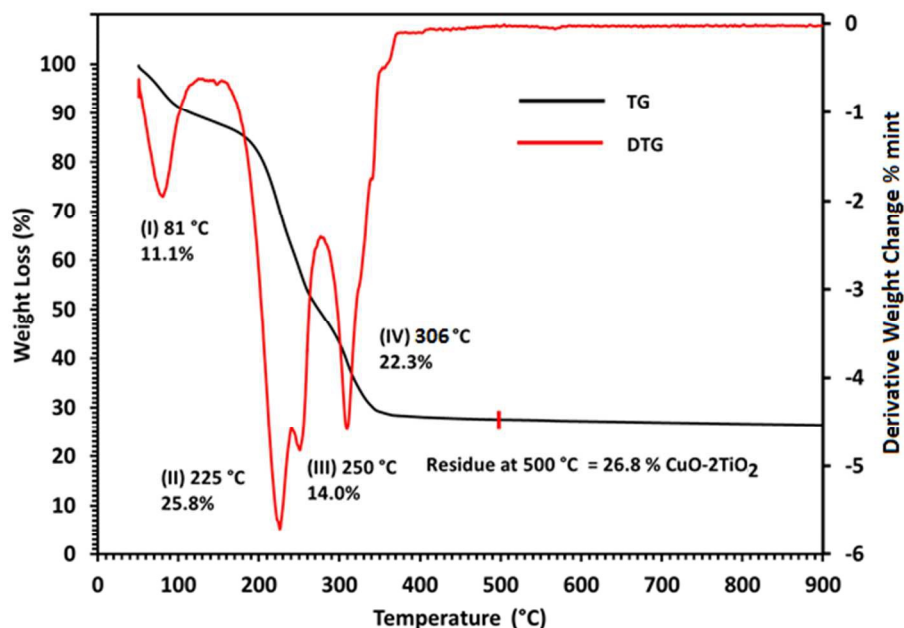


Figure 3: TG (black) and DTG (red) profiles representing thermal decomposition of complex (1) as a function of temperature.

3.4 Structural analysis

Thin films were developed via AACVD method on FTO glass substrate at temperature of 550 °C from 0.1M solution of precursor (1) in ethanol and methanol solvents respectively, using air as a carrier gas. The phase formation and degree of crystallinity of the deposited films were examined by XRD technique and X-ray diffractograms are comparatively overlapped in Figure 4. The XRD peak patterns seem identical in terms of their peak positions and 2θ values and both the diffractograms are dominated by the diffraction peak located at $2\theta = 25.27^\circ$ and 37.81° .

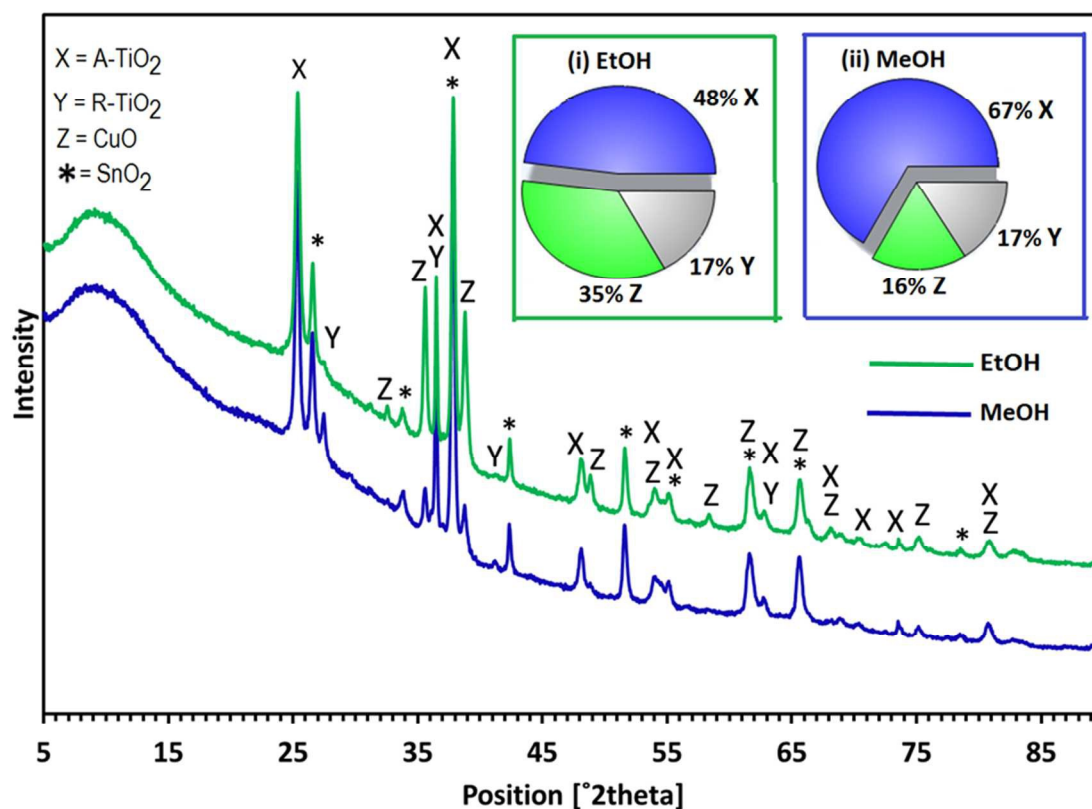


Figure 4: XRD patterns of the CuO-2TiO₂ composite thin films prepared from solutions of (1) in ethanol (green line), methanol (blue line), on FTO glass at 550 °C in air ambient; Inset shows the proportion of crystalline phases present in CuO-2TiO₂ composite films from (i) ethanol: 48% anatase TiO₂ (X), 17% rutile TiO₂ (Y), 35% tenorite TiO₂ (Z); (ii) methanol: 67% anatase TiO₂ (X), 17% rutile TiO₂, (Y) 16% tenorite CuO (Z).

XRD qualitative phase analysis was performed on each XRD pattern shown in Figure 4, which reveals the growth of tenorite CuO (ICSD 98-001-6025)³⁶ and a mixture of anatase (98-000-9853)³⁷ and rutile (98-003-1321)³⁸ TiO₂ phases as crystalline end product in both the cases. The prepared CuO exists in a monoclinic crystal system with space group C12/c1 and produced characteristic peaks indicated by (Z) at $2\theta = 32.58, 35.60, 48.84, 58.36,$ and 75.16° as observed by their Miller indices (110), (11-1), (20-2), (202) and

(004) respectively. The emergence of peaks at $2\theta = 25.27$ (011), 37.80 (112), 48.0 (020), 70.39 (220) and 73.59° (017) denoted by (X) are well indexed to tetragonal anatase TiO_2 . Furthermore, the peaks marked by (Y) at $2\theta = 27.46$ (110), 36.0 (011) and 41.27 (111) are attributed to tetragonal rutile TiO_2 . The X-ray diffractograms also demonstrate the overlapped peaks between CuO and anatase TiO_2 phases at 2θ values of 53.95 , 68.89 and 80.62° . A few common reflections originating from both anatase and rutile TiO_2 phases appear at 2θ values of 36.45 and 62.75° . No possible crystalline impurities such as metallic copper or Cu_2O were detected from these XRD patterns.

The XRD qualitative phase analysis has established that both the copper oxide-titania composite films deposited from two different solvents are comprised of similar crystalline phases including tenorite CuO and a mixture of anatase and rutile TiO_2 . The proportion of crystallinity of each phase in the composite product was determined by XRD semi-quantification analysis. The crystalline composition of CuO-2TiO₂ deposit obtained from ethanol is poised at 48% anatase TiO_2 (X), 17% rutile TiO_2 (Y) and 35% tenorite CuO (Z), respectively (inset Figure 4(i)). The film deposited from methanol contains the crystalline contents of 67% anatase TiO_2 (X), 16% rutile TiO_2 (Y) and 17% tenorite CuO (Z), respectively (inset Figure 4(ii)).

The crystalline contents of the CuO-2TiO₂ films deposited from different solvents varies from each other which suggest that solvents play a vital role in decorating the crystalline phases of the films on substrate surface by AACVD and not just act as a transport medium. In aerosol deposition, solvents play an important role in the determination of the extent of a reaction. The precursor can react differently in various solvents in the gas phase which may lead to the formation of different intermediates and thus to different

phases of the deposit. There have been similar reports whereby a variety of solvents have been used to alter the phase composition of titania using sol-gel approach, spray pyrolysis and AACVD.^{39,40}

Further the structural analysis of CuO-2TiO₂ composites thin films deposited from two different solutions was carried out by Raman spectroscopy and results are displayed in Figure 5.

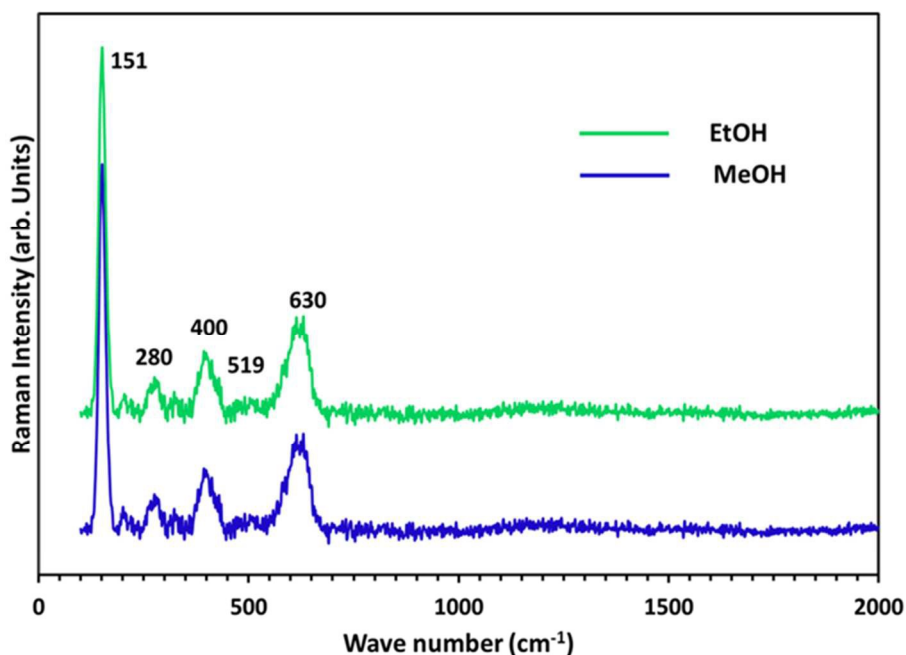


Figure 5 : Raman spectra of the CuO-2TiO₂ composite thin films prepared from solutions of (1) in ethanol (green line), methanol (blue line), on FTO glass substrate at 550 °C in air ambient.

The Raman scattering vibration modes detected at 151, 400, 519 and 630 cm⁻¹, corresponds to anatase TiO₂ phase⁴¹ and peaks located at 280 and 630 cm⁻¹ signify the presence of CuO phase.⁴² The characteristic peaks for rutile TiO₂ which are expected to appear at 246, 446 and 601 cm⁻¹ are merged in the broad bands at 280, 400 and 630 cm⁻¹.⁴³ Hence the CuO and mixture of anatase and rutile TiO₂ phases determined from our XRD analysis are further validated from Raman spectroscopy.

3.5 Micro-structural properties

The micro-structural properties of the films deposited from 0.1 M (20 mL) solution of precursor (**1**) in ethanol and methanol at 550 °C in air atmosphere were analysed by SEM. Figure 6 depicts the surface and cross sectional SEM images of CuO-2TiO₂ composite films. Figure 6(**a**) shows the surface topography of the film, prepared from ethanol solution, is composed of interconnected spherical objects of heterogeneous design, shape and size which are developed in the vertical direction of substrate plane. One type of microspherical object attains donuts shape structure while the other exists as round ball shaped entity of size range 0.5-1.3 μm (SI. Figure 2(**a2**)). The low resolution surface SEM images (SI. Figure 2(**a1**)) reveal that these microspherical objects are homogeneously distributed throughout the film matrix.

The cross sectional view of CuO-2TiO₂ composite film of average thickness 4.0 μm, deposited from ethanol solution, displayed in Figure 6(**b**) and (SI. Figure 2(**b1**)), show growth of small grains on the boundary layer of the FTO substrate. Figure 6 (**b**) shows that the surface architecture of the film obtained from methanol solution is made up of small and big sized spherical objects which are discretely grown in upward direction. The high resolution image (SI. Figure. 2(**c2**)) demonstrates that the surface of these spherical bodies is fully covered with buds. The low resolution surface SEM image (SI. Figure 2(**c1**)) depicts that these objects are uniformly furnished on substrate surface however the surface of the substrate is not fully covered as observed in the film deposited from ethanol solution.

The shape of the thin-film cross sections is shown in Figure 6(**d**) and (SI. Figure 2(**d1**)) and a layer of spheroid objects of thickness range 1.77-4.40 μm can be clearly seen on the surface of the FTO substrate.

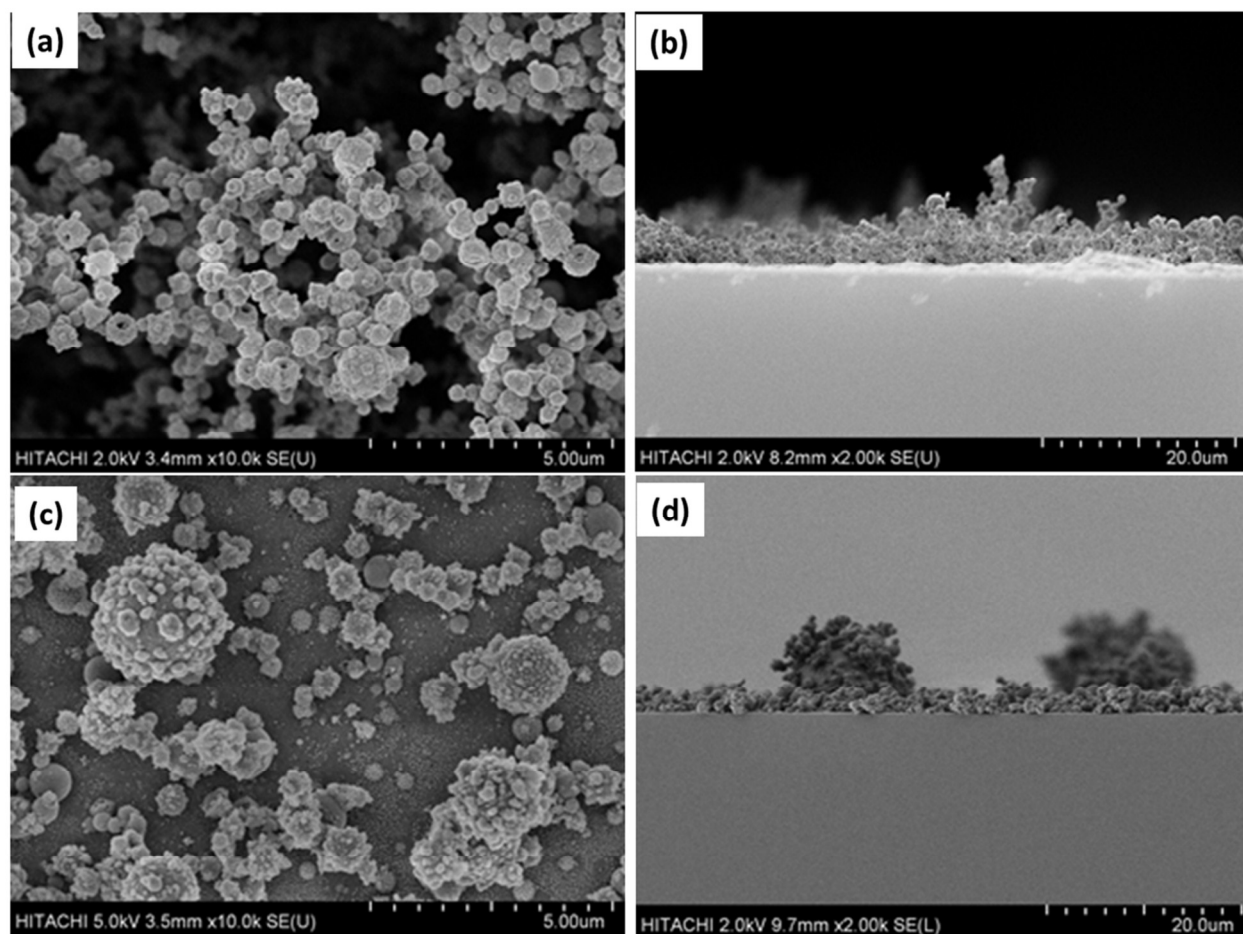


Figure 6: (a) and (c) show surface and (b) and (d) indicate the cross sectional SEM images of CuO-2TiO₂ composite thin films deposited on FTO glass substrate at 550 °C from solution of precursor (1) in (a, b) ethanol (c, d) methanol, respectively.

The elemental composition of CuO-2TiO₂ composite oxide thin films were analyzed by energy dispersive X-ray (EDX) analysis and spectra are presented in (SI. Figure 3 (a & b)). The EDX analysis executed on several randomly selected large regions reveal that the metallic ratio of Cu:Ti in the films is close to 1: 2 confirming the retention of the same metallic ratio in the films as found in complex (1).

Further EDX map analysis was performed to establish the composite nature of the CuO-2TiO₂ films. The distribution of the constituent Cu, Ti and O atoms has been highlighted by using

different color schemes as shown in SI. Figure 4 (a & b) which reveals the even distribution of these atoms throughout the films matrix.

3.6 XPS analysis

The XPS analysis was employed to determine the surface composition and chemical states of the Cu, Ti, and O elements in CuO-2TiO₂ composite oxide thin film prepared from ethanol solution of precursor (1) at 550 °C.

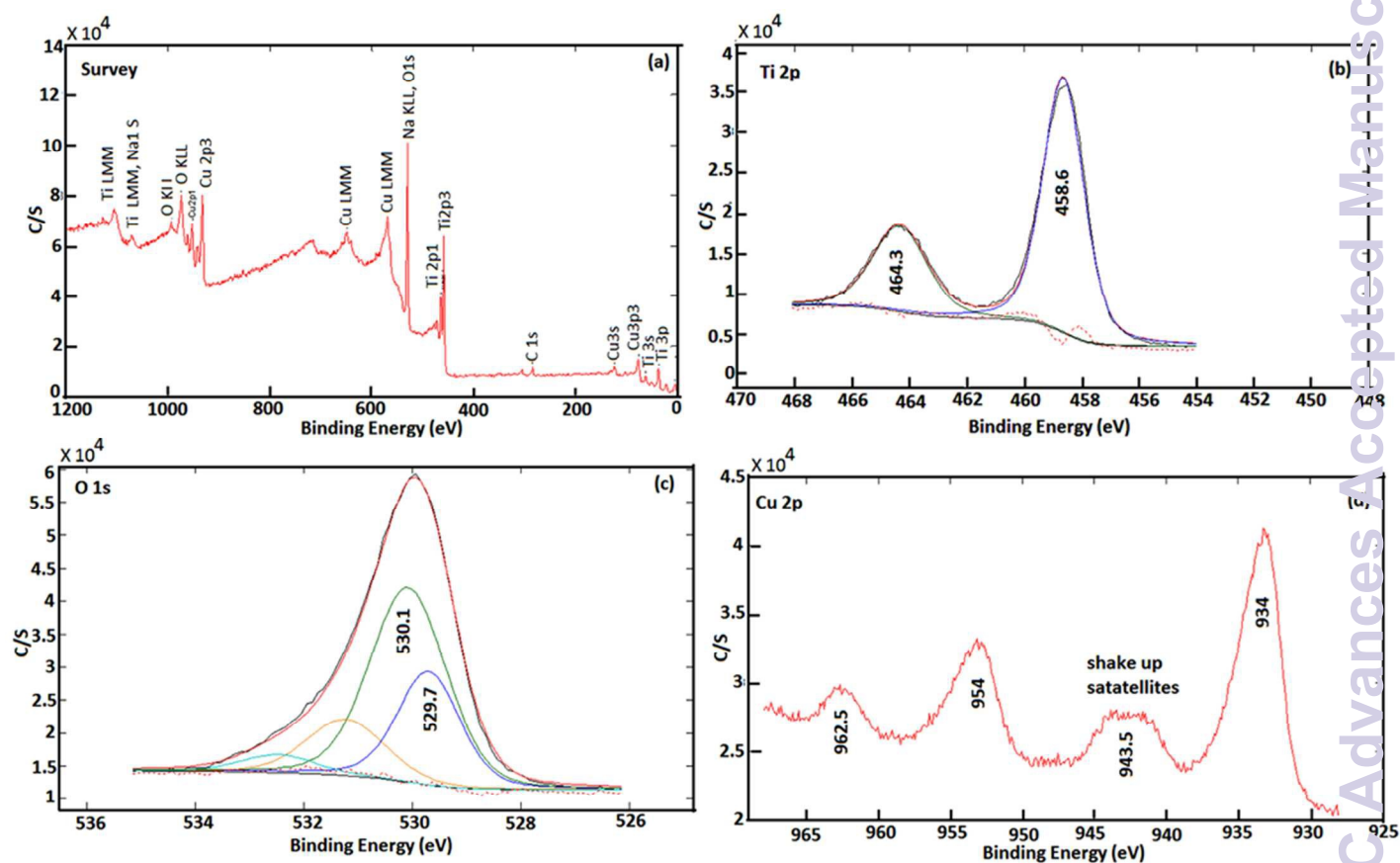


Figure 7: (a) Survey scan XPS spectrum of CuO-2TiO₂ composite thin films prepared from ethanol solution; High resolution spectra of CuO-2TiO₂ for (b) Ti 2p (c) O 1s (d) Cu 2p

The survey scan spectrum in Figure 7(a) shows the binding energy peaks at 458.4, 529.5 and 933.4 eV which are attributed to Ti 2p, O 1s and Cu 2p respectively. In the high resolution Ti 2p spectrum Figure 7(b), binding energies of 458.6 and 464.3 eV are indicative of Ti 2p_{3/2} and Ti

2p_{1/2} respectively which correspond to Ti⁴⁺ and matches well with the published data for TiO₂.¹⁶ Meanwhile, the peaks at 529.7 and 530.1 eV are evidence of O1s in CuO and TiO₂ Figure 7(c). The Cu 2p peak of the CuO-2TiO₂ is shown in Figure 7(d). The Cu 2p_{3/2} is allocated at 934 eV with a shakeup satellite peak at about 943.5eV and Cu 2p_{1/2} lies at 954 eV with a satellite peak at about 962.5eV, which is consistent with earlier reports.^{44,45} The presence of shakeup satellite features for Cu 2p rules out the possibility of presence of Cu₂O phase. The gap between Cu 2p_{1/2} and Cu 2p_{3/2} is 20eV, which is in agreement with the standard CuO spectrum.¹⁷

3.7 Electrochemical detection of nitrite ions by CuO-2TiO₂ film electrodes

The CuO-2TiO₂ composite film deposited from ethanol solution of (1) was used for the electrocatalysis and sensing of NO₂⁻ ions in 0.1 M phosphate buffer solution (PBS) (pH 7.2). The CuO-2TiO₂ composite electrode displayed an intense anodic peak current in the cyclic voltammogram for 5 mM NO₂⁻ at +1.0 V due to the electrocatalytic oxidation of NO₂⁻, Figure 8(b), and did not show any voltammetric response in the absence of NO₂⁻, Figure 8(a). During the electrocatalytic oxidation of NO₂⁻, two electrons were transferred and thus to form NO₃⁻ as a product.^{46,47}

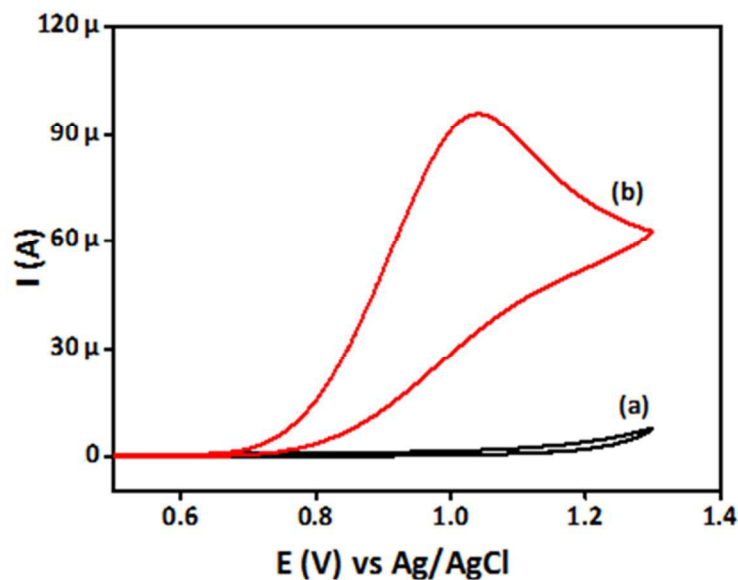


Figure 8: Cyclic voltammograms obtained for the CuO–2TiO₂ composite thin film in the (a) absence and (b) presence of 5 mM NO₂[−] ions in 0.1 M PBS (pH 7.2) at a scan rate of 50 mV s^{−1}

Further, influence of the scan rate on the electrocatalytic oxidation peak potential (E_{pa}) and peak current for NO₂[−] at the CuO–2TiO₂ film electrode in 0.1 M PBS (pH 7.2) were studied using CV, as shown in Figure 9(a). The current values were found to be increased with an increase in the scan rate from 10 to 300 mV s^{−1}, Figure 9(a). The linear relationship between the anodic peak currents and the square root of the scan rate is shown in Figure 9(b). As can be seen, the anodic peak current (I_{pa}) for the 1 mM NO₂[−] varied linearly with the square root of the scan rate ($v^{1/2}$), with a linear regression equation of I_{pa} (μA) = 0.205 $v^{1/2}$ + 20.48 and a correlation coefficient R^2 = 0.971. This result indicates that the electron transfer of the CuO–2TiO₂ composite film is mainly controlled by a diffusion-controlled electrochemical process.²⁷

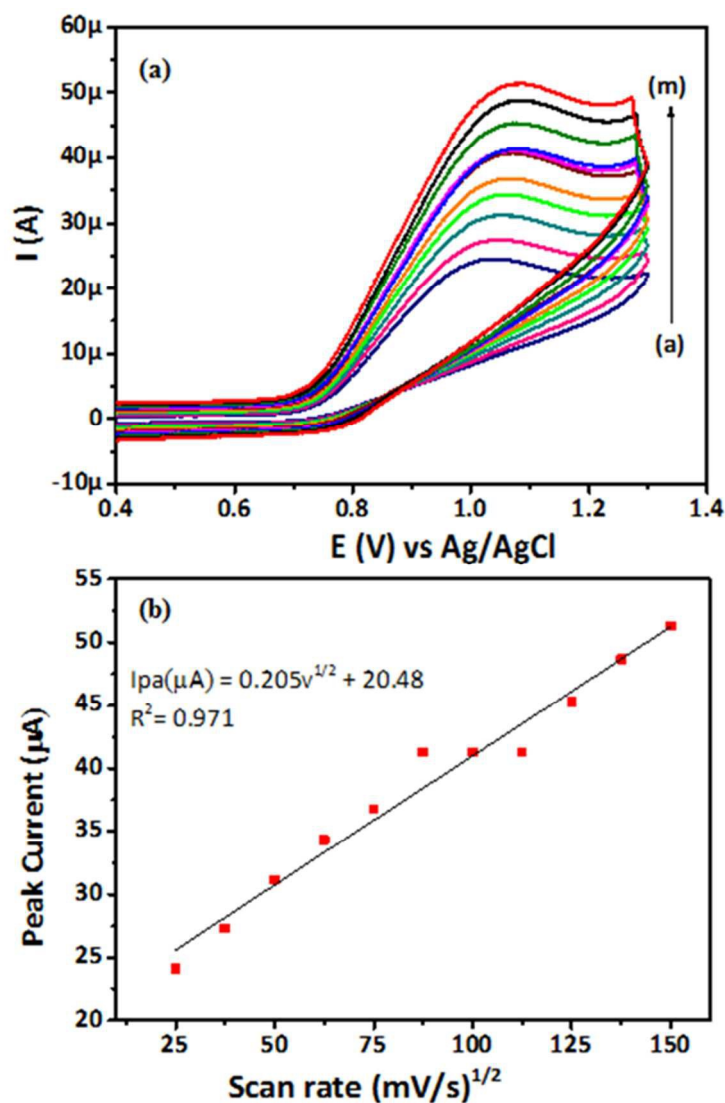


Figure 9: (a) Cyclic voltammograms recorded for the CuO-2TiO₂ electrode in the presence of 1 mM NO₂⁻ ions in 0.1 M PBS (pH 7.2) at various scan rates of ((a)-(m)) 10-300 mV s⁻¹. (b) Plot of anodic peak current vs square root of the scan rate obtained for the CuO-2TiO₂ electrode.

The sensitivity of the sensor under the optimized detection for NO₂⁻ conditions were tried, and a series of linear sweep voltammetry (LSV) curves were recorded in 0.1 M PBS (pH 7.2) with different NO₂⁻ concentrations at the CuO-2TiO₂ electrode as shown in Figure 10(a). It could be observed that the anodic peak current increased linearly with an increase in the concentration of

NO_2^- in the range of 10 to 200 μM , with a linear regression equation of $I_{\text{pa}} = 0.0415 \text{ M} + 1.4336 \mu$ ($R^2 = 0.9994$), Figure 10(b). The sensitivity is determined from the slope of the calibration plot. The Figure 10(b) shows the standard addition line, limit of detection (LoD) for NO_2^- was calculated as 16.6 nM ($S/N = 3$). It can be seen that this present detection limit is comparable as well as lower than detection limits obtained for other oxides by different electrochemical methods.

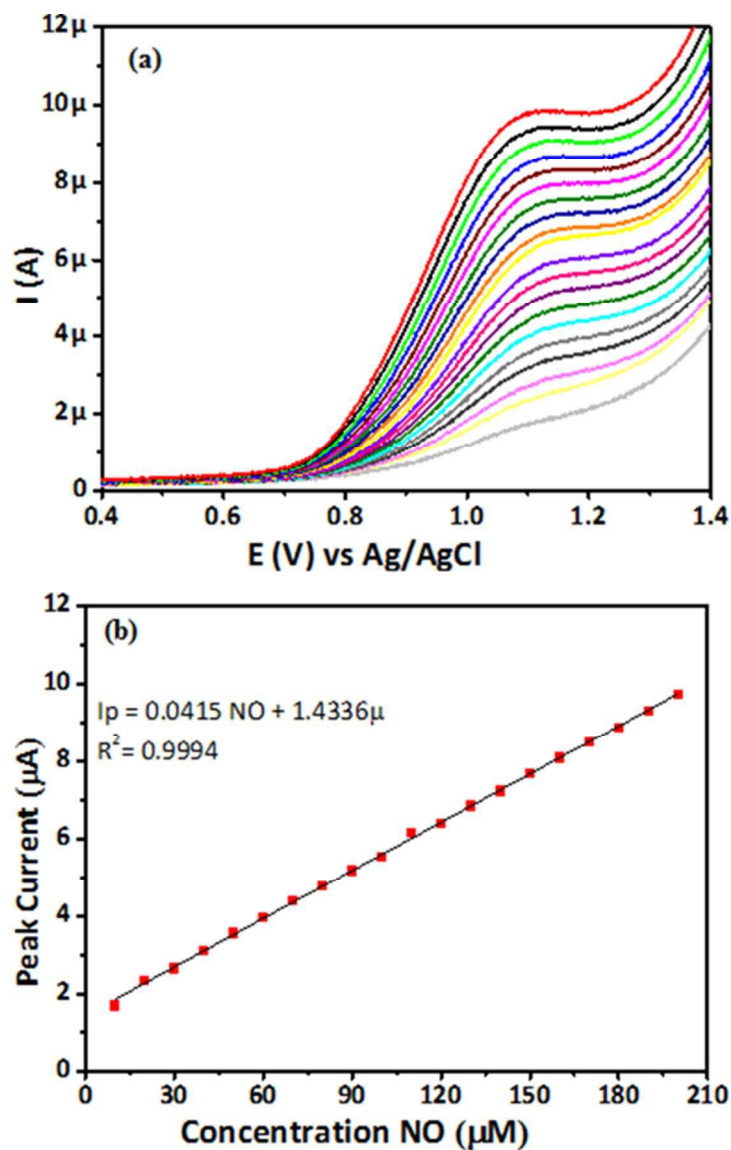


Figure 10: (a) Linear sweep voltammograms (LSV) obtained for the CuO–2TiO₂ composite thin film for various concentration of NO₂⁻ ions in 0.1 M PBS (pH 7.2) at a scan rate of 50 mV s⁻¹. (b) Correlation between the concentration of NO₂⁻ and peak current for the CuO–2TiO₂ electrode.

The sensing performance of the CuO–2TiO₂ composite film was compared with other previously reported sensor materials for the detection of NO₂⁻ and the results are summarized in Table 3 which indicates that the detection limit of the present sensor is better than the other oxide materials.

Table 3: Comparison of analytical performance of various electrochemical sensors for nitrite (NO₂⁻) detection.

Sensor material	Analytical technique	Limit of detection (LOD) μM	Ref.
MnO ₂ -CP-E	Linear sweep voltammetry	1.2	⁴⁸
Cobalt oxide	Cyclic voltammetry	20,000	⁴⁹
CuO–graphite	Cyclic voltammetry	0.6	⁵⁰
PbO ₂ – graphite	Cyclic voltammetry	0.9	⁵¹
<i>f</i> -ZnO@rFGO	Linear sweep voltammetry	33	⁴⁷
ZnTiO ₃ –TiO ₂	Amperometry	3.98	³⁴
CuO–2TiO ₂	Linear sweep voltammetry	0.0166	Present work

The selectivity of the CuO–2TiO₂ electrode for the determination of NO₂⁻ investigated by adding various possible interferents and observing the change in current (Figure 11). The LSV was continuously recorded for the addition of common interferents such as NaF, NH₄Cl, KCl, NaNO₃ and MgSO₄ in a homogeneously stirred of 0.1 M PBS (pH 7.2) and there is no significant current response found due the interferents. Upon addition 100 μM NO₂⁻, the electrode showed the response signal (Figure 11). This observation clearly demonstrates that the selective detection of NO₂⁻ even in the presence of common interferents is possible and the CuO–2TiO₂ composite possesses high selectivity toward NO₂⁻ over other common interferents.

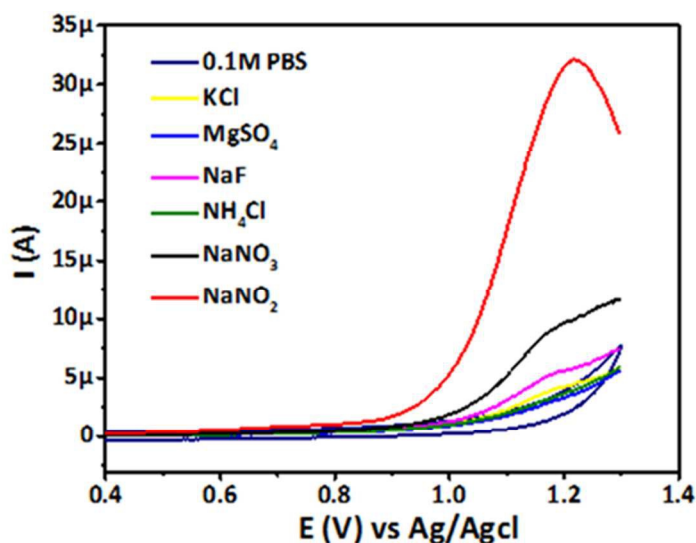


Figure 11: LSV response obtained for CuO–2TiO₂ composite thin film for the addition of and each 1000 μM addition of other interferences such as KCl, MgSO₄, NaF, NH₄Cl, NaNO₃ and 100 μM NO₂⁻ ions in 0.1 M PBS (pH 7.2) at scan rate of 50 mV s⁻¹.

4 Conclusions

In summary, a synthetic procedure for the preparation of heterobimetallic complex [Cu₂Ti₄(O)₂(OH)₄(TF)₈(THF)₆]·THF (**1**), by reacting copper (II) acetate with titanium (IV)

isopropoxide in the presence of trifluoroacetic acid in tetrahydrofuran, and its structural characterization has been presented. The thermolysis behaviour of the complex indicates its clean thermal decomposition at relatively low temperature of 500 °C. The high solubility of complex (1) in ethanol and methanol makes it proficient as a molecular precursor for the growth of CuO-2TiO₂ composite oxide thin films on FTO conducting glass substrate by aerosol assisted chemical vapour deposition method. Scanning electron microscopic images indicate that the size, shape and textures of microspherical architectures of the composite oxides films are greatly influenced by the type of deposition solvent used. The fabricated films have been found to comprise copper oxide: titania phases in (1: 2). Applicability of fabricated CuO-2TiO₂ electrode in electrochemical sensor was investigated towards the detection of NO₂⁻ ions and the electrode showed the limit of detection (LoD) of 0.0166 μM with linear range of 10 to 200 μM. Beyond this, present sensor electrode is more selective towards NO₂⁻ ions in the presence of other common interfering species. This CuO-2TiO₂ electrode is more suitable for the selective and sensitive detection of toxic NO₂⁻ ions from environmental remediation aspect.

Supplementary data

CCDC 1442375 contains the supplementary crystallographic data for this paper. These data can be obtained free of charge from The Cambridge Crystallographic Data Centre via www.ccdc.cam.ac.uk/data_request/cif.

Electronic Supplementary Information (ESI) available: [SEM images, Energy dispersive X-ray spectra and single crystal X-ray crystallography]. See DOI: 10.1039/b000000x/

Acknowledgements

The authors acknowledge the High-Impact Research scheme grant number: UM.C/625/1/HIR/242, UMRG scheme grant number: RP007-13AET and HIR-MOHE grant number: UM.S/P/628/3SC21 for funding.

References

1. M. D. Newman, M. Stotland and J. I. Ellis, *J. Am. Acad. Dermatol.*, 2009, **61**, 685-692.
2. X. Chen and S. S. Mao, *Chem. Rev.*, 2007, **107**, 2891-2959.
3. A. Kudo and Y. Miseki, *Chem. Soc. Rev.*, 2009, **38**, 253-278.
4. X. Chen and A. Selloni, *Chem. Rev.*, 2014, **114**, 9281-9282.
5. Z. F. Yin, L. Wu, H. G. Yang and Y. H. Su, *Phys. Chem. Chem. Phys.*, 2013, **15**, 4844-4858.
6. K. Harrison, J. Levene, K. Rajeshwar, R. McConnell and S. Licht, *Electrolysis of water. New York: Springer Inc, 2008, 41-64.*
7. J. Zhang, J. H. Bang, C. Tang and P. V. Kamat, *ACS Nano*, 2009, **4**, 387-395.
8. Q. Yan, J. Wang, X. Han and Z. Liu, *J. Mater. Res.*, 2013, **28**, 1862-1869.
9. M. S. Hassan, T. Amna, H. Y. Kim and M.-S. Khil, *Compos. Part B: Eng.*, 2013, **45**, 904-910.
10. Y. Cai, Y. Ye, Z. Tian, J. Liu, Y. Liu and C. Liang, *Phys. Chem. Chem. Phys.*, 2013, **15**, 20203-20209.
11. S. E. Stanca, R. Müller, M. Urban, A. Csaki, F. Froehlich, C. Krafft, J. Popp and W. Fritzsche, *Catal. Sci. Tech.*, 2012, **2**, 1472-1479.
12. M. Logar, B. t. Jančar, S. o. Šturm and D. Suvorov, *Langmuir*, 2010, **26**, 12215-12224.
13. J. Yu, Y. Hai and M. Jaroniec, *J. Colloid Interface Sci.*, 2011, **357**, 223-228.
14. S. S. Lee, H. Bai, Z. Liu and D. D. Sun, *Water Res.*, 2013, **47**, 4059-4073.
15. A. Yousef, N. A. Barakat, T. Amna, S. S. Al-Deyab, M. S. Hassan, A. Abdel-hay and H. Y. Kim, *Ceram. Int.*, 2012, **38**, 4525-4532.
16. S. S. Lee, H. Bai, Z. Liu and D. D. Sun, *Appl. Catal., B*, 2013, **140**, 68-81.
17. L. Zhu, M. Hong and G. W. Ho, *Nano Energy*, 2015, **11**, 28-37.
18. M. Shahid, M. Mazhar, A. A. Tahir, M. K. Rauf and J. Raftery, *Aust. J. Chem.*, 2014, **67**, 757-762.
19. M. A. Ehsan, H. Khaledi, A. Pandikumar, N. M. Huang, Z. Arifin and M. Mazhar, *J. Solid State Chem.*, 2015, **230**, 155-162..
20. M. A. Ehsan, H. Khaledi, Z. Arifin and M. Mazhar, *Polyhedron*, 2015, **98**, 190-195.
21. A. A. Tahir, M. Hamid, M. Mazhar, M. Zeller, A. D. Hunter, M. Nadeem and M. J. Akhtar, *Dalton Trans.*, 2008, 1224-1232..
22. M. Hamid, A. A. Tahir, M. Mazhar, M. Zeller and A. D. Hunter, *Inorg Chem.*, 2007, **46**, 4120-4127.
23. W. D. Buchanan and K. Ruhlandt-Senge, *Chem. Eur. J.*, 2013, **19**, 10708-10715.

24. P. C. Andrews, P. C. Junk, I. Nuzhnaya and L. Spiccia, *Dalton Transactions*, 2008, 2557-2568.
25. W. D. Buchanan, M. A. Guino-o and K. Ruhlandt-Senge, *Dalton Trans.*, 2008, 2557-2568.
26. A. Pandikumar, S. Manonmani and R. Ramaraj, *Catal. Sci. Tech.*, 2012, **2**, 345-353.
27. N. I. Ikhsan, P. Rameshkumar, A. Pandikumar, M. M. Shahid, N. M. Huang, S. V. Kumar and H. N. Lim, *Talanta*, 2015, **144**, 908-914.
28. L. Krause, R. Herbst-Irmer, G. M. Sheldrick and D. Stalke, *J. Appl. Cryst.*, 2015, **48**, 3-10.
29. G. M. Sheldrick, *Acta Cryst.*, 2015, **A71**, 3-8.
30. G. M. Sheldrick, *Acta Cryst.*, 2015, **C71**, 3-8.
31. C. R. Hubbard, E. Evans and D. Smith, *Journal of applied crystallography*, 1976, **9**, 169-174.
32. C. R. Hubbard and R. L. Snyder, *Powder Diffraction*, 1988, **3**, 74-77.
33. R. L. Snyder, *Powder Diffraction*, 1992, **7**, 186-193.
34. M. A. Ehsan, H. Khaledi, A. Pandikumar, P. Rameshkumar, N. M. Huang, Z. Arifin and M. Mazhar, *New J. Chem.*, 2015, **39**, 7442-7452.
35. M. A. Ehsan, A. A. Tahir, M. Hamid, M. Mazhar, K. U. Wijayantha and M. Zeller, *Inorg. Chim. Acta*, 2011, **376**, 189-194.
36. S. Åsbrink and L.-J. Norrby, *Acta Cryst.*, 1970, **B26**, 8-15.
37. E.P. Meagher, C.F. Schwerdtfeger, M. Horn, , Wroclaw, , *Golden Book of Phase Transitions*, 2002, **1**, 1 - 123.
38. W. Gonschorek., *Golden Book of Phase Transitions, Wroclaw*, 2002, **1**, 1-123.
39. C. Edusi, G. Sankar and I. P. Parkin, *Chem. Vap. Deposition*, 2012, **18**, 126-132.
40. L. Xiaoxin, J. Zhengguo, B. Shaojing and Y. Tao, *J. Sol-Gel Sci. Technol.*, 2005, **36**, 103-111.
41. N. T. Nolan, M. K. Seery and S. C. Pillai, *Chem. Mater.*, 2011, **23**, 1496-1504.
42. T. H. Nguyen, T. L. Nguyen, T. D. T. Ung and Q. L. Nguyen, *Advances in Natural Sciences: Nanoscience and Nanotechnology*, 2013, **4**, 025002.
43. F. Hardcastle, *J Ark Acad Sci*, 2011, **65**, 43-48.
44. M. A. Dar, S. H. Nam, Y. S. Kim and W. B. Kim, *J. Solid State Electr.*, 2010, **14**, 1719-1726.
45. D. Tahir and S. Tougaard, *J. Phys. Condens. Matter.*, 2012, **24**, 175002.
46. R. Guidelli, F. Pergola and G. Raspi, *Anal. Chem.*, 1972, **44**, 745-755.
47. A. Pandikumar, N. Yusoff, N. M. Huang and H. N. Lim, *Microchim. Acta*, 2014, **182**, 1113-1122.
48. C. E. Langley, B. ŠLJUKIC, C. E. Banks and R. G. Compton, *Anal. Sci.*, 2007, **23**, 165-170.
49. A. Salimi, R. Hallaj, H. Mamkhezri and S. M. T. Hosaini, *J. Electroanal. Chem.*, 2008, **619**, 31-38.
50. B. Šljukić, C. E. Banks, A. Crossley and R. G. Compton, *Electroanalysis*, 2007, **19**, 79-84.
51. B. Šljukić, C. E. Banks, A. Crossley and R. G. Compton, *Anal. Chim. Acta* 2007, **587**, 240-246.

Graphical Abstract

An electrochemical nitrite ions sensor electrode, CuO-2TiO₂, has been developed using single molecular precursor [Cu₂Ti₄(O)₂(OH)₄(TF)₈(THF)₆]·THF in aerosol assisted chemical vapour deposition technique.

